

Optimization of an advanced battery model parameter minimization tool and development of a novel electrical model for lithium-ion batteries

Noshin Omar*,†, Dhammadka Widanage, Mohamed Abdel Monem, Yousef Firouz, Omar Hegazy, Peter Van den Bossche, Thierry Coosemans and Joeri Van Mierlo

Vrije Universiteit Brussel, Pleinlaan 2, Brussel, 1050, Belgium

SUMMARY

This paper represents the optimization of an advanced battery model parameter minimization tool for estimation of lithium-ion battery model parameters. This system is called extended Levenberg–Marquardt. The proposed system is able to predict the nonlinearity of lithium-ion batteries accurately. A fitting percentage of over 99% between the simulation and experimental results can be achieved.

Then, this paper contains a new second-order electrical battery model for lithium-ion batteries, extracted on the basis of experimental study and able to predict the battery behavior precisely.

Further, in this paper, an extended comparative study of the performances of the various existing electrical battery models in the literature (R_{int} , RC, Thévenin, and FreedomCar) for lithium-ion batteries against the new developed battery model is presented, on the basis of the optimized battery parameter minimization tool.

These battery models have been validated at different working conditions. From the analysis, one can observe that the new proposed battery model is more accurate than the existing ones and that it can predict the battery behavior during transient and steady-state operations.

Finally, the new battery model has been validated at different working temperatures. The analysis shows that the error percentage between 0% and 90% depth of discharge at 40 °C is less than 1.5% and at 0 °C less than 5%. Copyright © 2013 John Wiley & Sons, Ltd.

KEY WORDS: battery models; Thévenin; FreedomCar; new battery model; Levenberg–Marquardt; validation; HPPC test

1. INTRODUCTION

As the global economy begins to strain under the pressure of rising petroleum prices and environmental concerns, research have spurred into the development of various types of clean energy transportation systems such as hybrid electric vehicles (HEVs), battery electric vehicles (BEVs), and plug-in HEVs (PHEVs) [1–5]. In urban traffic, due to their beneficial effects on environment, electric vehicles are an important factor for improvement of traffic and more particularly for a healthier living environment. Especially, PHEVs acquire the most attention due to the combination of an electrical source and a conventional engine. This type of vehicle provides the user a considerable pure electrical range and also an extended range, which can be performed by a conventional internal combustion engine. The establishment of a rechargeable energy storage system that can support the output power during acceleration, efficiently use the regenerative energy, and perform for a considerable life cycle are the critical aspects to be met by battery technologies [6–12].

Furthermore, the individual battery cells making up the battery in BEVs, PHEVs, and HEVs are not identical, and therefore, there is a need for a battery management system (BMS) whereby the individual battery cells should be continuously balanced to avoid big variations between the cells, in order to

*Correspondence to: Noshin Omar, Vrije Universiteit Brussel, Pleinlaan 2, Brussel, 1050, Belgium.

†E-mail: noshomar@vub.ac.be

extend the battery lifetime and the vehicle range [10,13,14]. The BMS keeps the battery cells into its safe operation area by avoiding thermal runaway and irregular discharging and/or charging.

Battery management systems are highly dependent on accurate battery models. The model should be able to predict the static and dynamic behaviors of the cell. In PHEVs, the battery model also should have good prediction capability under all conditions such as a wide state-of-charge (SoC) window and temperature range. Further, the model should have a good response during transient and steady-state periods.

In the last decade, extensive research has been performed on the development of various battery models for different purposes. These models can be divided into three main categories:

- Electrochemical battery models.
- Mathematical battery models.
- Electrical battery models.

In this section, an overview over these battery models is presented. The merits and drawbacks of each battery model are analyzed. Moreover, the estimation techniques of the proposed models are also compared.

1.1. Electrochemical battery models

For analyzing the electrochemical behavior of the batteries, many models have been proposed by electrochemical experts [15–30]. The first electrochemical models were developed for lead–acid, nickel cadmium and nickel metal-hydride batteries, with a considerable effort having been made during the last years for lithium-ion batteries. These models are particularly appropriate to simulate the ions transfer between the electrodes and to study some specific phenomena on electrode and electrolyte level.

In [15], an electrochemical lithium-ion model is developed for the evaluation of the capacity fade during charging and discharging based on the loss of the active lithium-ion material. In [27], the authors developed an electrochemical model for the prediction of the battery behavior. The model has been built on the basis of electrochemical relationships. The author considered the chemical reactions in the battery and the ion transfer between the electrodes. This model makes use of impedance spectroscopy for characterization of the battery model parameters. In [28], the authors modeled the effect of the anode resistance on the lithium-ion battery abilities during charging and discharging. The developed model requires very specific parameters such as particle radius, specific surface area of the porous electrode, solid phase concentration of lithium, and diffusion coefficient. In [19], a lithium-ion bond graph model is presented. The model uses electrochemical laws to illustrate the energy effect at a macroscopic scale at electrode and at electrolyte level.

According to these electrochemical models, a considerable high number of chemical parameters and a thorough knowledge of the different material properties are required. In addition, the proposed models are based on well specific test profiles at low current rates (in the range of milliampere). Moreover, the model parameters can only be extracted by performing dedicated chemical tests. These models tend to be time-consuming, cumbersome, and complex for practical applications [15–28].

1.2. Mathematical battery models

Mathematical battery models are extensions of the electrochemical battery models that describe the mass transport and thermodynamics phenomena in the battery. The models need many relationships related to all battery components. Mostly, these models use first-order and second-order partial differential equations. Because of the complexity of the models, dedicated mathematical techniques or estimation tools are required for solving the model equations [31–33]. However, the difference between the mathematical and electrochemical in the scientific world is not clear yet.

In [34], a mathematical model is developed to illustrate the effect of intercalation and oxygen reactions in nickel–cadmium-based batteries. The model predicts the battery discharge and charge voltage. According to the model, the positive electrode causes the generated oxygen, which is electrochemically reduced in the negative electrode.

In [35], a model is presented, which describes the discharge performances of Li_xTiS_2 -based battery. The effect of the electrode geometry on the discharge current is studied. In order to simulate the

lithium-ion-based battery performances with a small error percentage, an analytical model is proposed in [36] for prediction of the remaining battery capacity. Then, the model can be used for online measurements purposes. It also describes the temperature and life cycle effects by imposing a load current. The model has been validated, and the accuracy is about 5%. However, the model requires many electrochemical relationships, which make the model very complicated and useless in BMS of PHEV applications.

In [37,38], mathematical models are described on the basis of chemical kinetic process in the battery, making use of the ‘two wells’ approach. However, these models are not able to describe the battery cell voltage response when applying a load.

1.3. Electrical battery models

Compared with electrochemical and mathematical battery models, the electrical battery models describe the battery behavior by means of an electrical equivalent scheme consisting of components such as resistors, capacitors, inductors, and diodes. Because of their high integration capabilities, the models could be integrated in any BMS, which makes them the appropriate model approach for diagnostics issues. Furthermore, the model parameters can be extracted by assuming the battery as an electrical network. This removes the need to perform specific electrochemical characterization tests on the internal parts of the battery, as it is the case for the two previous model approaches.

1.3.1. Models from literature. In the following section, some models found in literature are cited. The most relevant electrical models in the literature are compared and analyzed in the following subsections.

In [39], an electrical model is presented on the basis of the Shepherd equation. This is an empirical relationship, which describes the battery behavior in terms of terminal voltage, open circuit voltage (OCV), internal resistance, current rate, and SoC. The Shepherd model indicates good performances at constant load (>2% error). But the dynamic behavior of the model is poor (>10% error). The battery model in the MATLAB/Simulink, SimPowerSystem toolbox is based on the Shepherd model.

In order to increase the dynamic performance of the Shepherd model, in [40], a new battery model approach consisting of several Resistor-capacitor (RC) circuits is proposed. Their main focus was to demonstrate the relaxation effect in lithium-ion batteries. They concluded that the battery accuracy increases if more RC circuits are introduced in the model. However, this also increases the computational time and complexity of the model. In [41], an enhanced Thévenin model of lead-acid batteries for use in domestic fuel cell systems is proposed. The ohmic resistance in the original Thévenin model has been adapted to separate charge and discharge resistances. Moreover, the RC circuit has been modified by two resistances (R_{co} and R_{do}) representing the charge and discharge polarization resistances. A self-discharge resistance has also been added. The model seems accurate by employing constant currents. But the dynamic behavior of the model in PHEVs and particularly for lithium-ion batteries has not been proven. In [42], a third-order battery model for lead-acid batteries is developed. The battery model consists of two RC circuits and one algebraic parasitic branch. The main parameters of the branches are in function of SoC and of temperature. The relationships for the model parameters have been derived from experimental results. However, the applicability of this model has only been proven for lead-acid batteries.

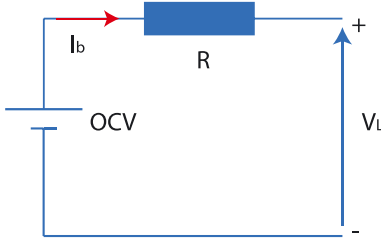
1.3.1.1. R_{int} battery model. The simplest electrical model considers the battery as a voltage source with an internal resistance. This elementary model can be sophisticated by considering its parameters (such as OCV and internal resistance (R)) as a function of SoC and temperature. This approach has been used in the ‘advisor’ simulation tool [43,44] and is presented in Figure 1. Moreover, the internal resistance is also considered as a function of the battery current flow [45].

According to Figure 1, the battery voltage can be considered as follows:

$$V_L = \begin{cases} OCV - R_d \cdot I_b & \text{if } I_b > 0 \text{ (discharge)} \\ OCV - R_{ch} \cdot I_b & \text{if } I_b < 0 \text{ (charge)} \end{cases} \quad (1)$$

where

- V_L : battery voltage (V),
- OCV : open circuit voltage (V),

Figure 1. R_{int} battery model.

- R_d : discharge internal resistance (Ω),
- R_{ch} : charge internal resistance (Ω), and
- I_b : battery current (A).

The R_{int} model has the advantage that the model is not complicated and easily can be integrated in any BMS. However, the model in the present form is not appropriate to predict the battery behavior accurately [45].

1.3.1.2. RC battery model. In 2000, Saft Company provided the National Renewable Energy Laboratory a battery model specific for high power applications [45]. The model is illustrated in Figure 2. The model can be described by the state-space equation as presented by Equation (2)

$$\begin{pmatrix} \dot{V}_{cb} \\ \dot{V}_{cc} \end{pmatrix} = \begin{pmatrix} \frac{1}{C_b(R_e + R_c)C_b(R_e + R_c)} & \frac{1}{C_b(R_e + R_c)} \\ \frac{1}{C_{cc}(R_e + R_c)} & -\frac{1}{C_{cc}(R_e + R_c)} \end{pmatrix} \begin{pmatrix} V_{cb} \\ V_{cc} \end{pmatrix} + \begin{pmatrix} -\frac{R_c}{C_b(R_e + R_c)} \\ -\frac{R_c}{C_c(R_e + R_c)} \end{pmatrix} I_b \quad (2)$$

$$V_o = \left(\frac{R_c}{R_e + R_c R_e + R_c} \right) \begin{pmatrix} V_{cb} \\ V_{cc} \end{pmatrix} + \left(R_t - \frac{R_c \cdot R_e}{R_e + R_c} \right) I_b$$

where

- C_b : bulk capacitor (F),
- C_s : surface capacitor (F),
- R_e : resistance in series with the capacitor C_b (Ω),
- R_c : resistance in series with capacitor C_c (Ω),
- R_t : represents the resistance of the connection between the two RC circuits (Ω),
- V_{cc} : voltage over the capacitor C_c (V),
- V_{cb} : voltage over the capacitor C_b (V),
- I_b : current through the battery (A).

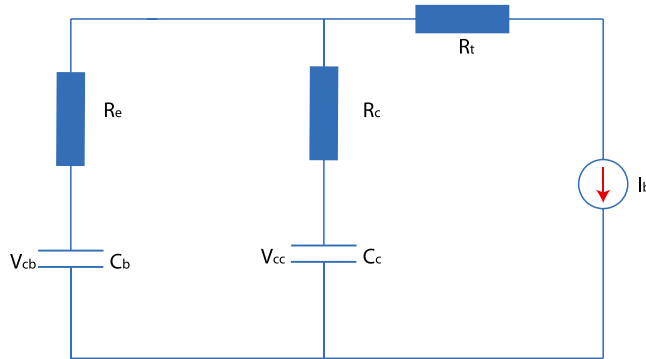


Figure 2. RC battery model [43].

As it is shown in Figure 2, the model consists of two capacitors (C_b , C_c) and three resistors (R_e , R_c , R_t). The capacitor C_c represents the surface phenomena, which has a small value and is called surface capacitor [41]. The bulk capacitor C_b has a very large value and describes the battery abilities to store charge chemically [45].

The SoC of the model is based on the voltage change over the capacitor C_b . However, unlike electrical double-layer capacitor, the battery voltage of high power lithium-ion batteries is not linear in function of depth of discharge as reported in [10]. Here, it should be noted that the parameters of the battery model are fixed and cannot vary in function of SoC or temperature [45]. The latter is clearly a disadvantage.

1.3.1.3. FreedomCar battery model. In Figure 3, the model represented by FreedomCar (also known as partnership for a new generation of vehicles is presented [46]. The model consists of an OCV, an ohmic resistance R_o , a polarization resistance (due to the concentration gradient) R_p , a fictive capacitor ($1/OCV'$), which represents the capacitance that accounts the variation in OCV with the time integral of the load current I_b , and a capacitor C , which describes the battery behavior during transient phases. On the basis of the Kirchoff Voltage law, the voltage of the battery can be calculated when a load is imposed as presented by Equation (3). This equation forms the basis of the FreedomCar battery parameter estimation spreadsheet (see Figure 4). The proposed estimation method needs the load current I_b , battery voltage V_L , and the time vector T . According to these input vectors, the battery model parameters can be estimated. In order to estimate the model parameters, the regular hybrid pulse power characterization (HPPC) test at every 10% SoC value should be carried out. The HPPC test consists of 10-s discharge and charge pulses at maximum discharge load and 0.75 of the maximum discharge load, respectively, as can be seen in Figure 5. The proposed HPPC test is also applicable for the RC battery model. Here, it should be underlined that the polarization current I_p through the resistance R_p can be obtained on the basis of the differential Equation (4), with an initial condition $I_p=0$ at $t=0$.

$$V_L(t) = OCV(t) - OCV'(t)\int I_b(t).dt - R_o.I_b(t) - R_p.I_p(t) \quad (3)$$

$$\frac{dI_p}{dt} = \frac{I_b - I_p}{\tau} \quad (4)$$

The solution of Equation (4) in discrete form is given by Equation (5)

$$I_{p,i} = \left(1 - \frac{1 - e^{-\Delta t/\tau}}{\Delta t/\tau}\right).I_{b,i} + \left(\frac{1 - e^{-\Delta t/\tau}}{\Delta t/\tau} - e^{-\frac{\Delta t}{\tau}}.I_{b,i} + e^{-\frac{\Delta t}{\tau}}.I_{p,i-1}\right) \quad (5)$$

where

- $1/OCV'$: fictive capacitor (F),
- R_p : polarization resistance (Ω),

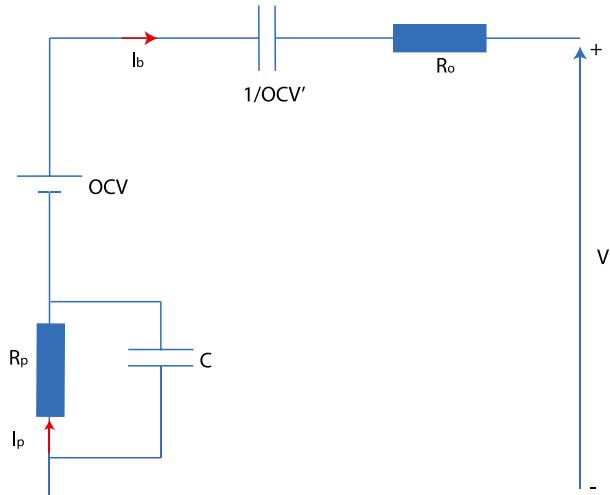


Figure 3. Partnership for a new generation of vehicles [44].

HPPC Battery Parameter Estimator Spreadsheet

Column 1	Column 2	Column 3	Column 4	Column 5	Col 6	Col 7	Col 8	Col 9	Col 10	Col 11	Col 12
dT/tau	Time [s]	I load [A]	I _p [A]	SOC [As]	"Voltage"	Est V load [V]	V error [V]	Tau	R2		
0,00	0,02	245,07	0,23	2,21	3,47	3,48	0,02	9,5	0,999		
0,11	1,02	244,98	24,79	248,31	3,47	3,47	0,00				
0,11	2,02	244,98	46,81	493,49	3,45	3,45	0,00				
0,10	3,02	244,99	66,56	737,79	3,43	3,44	0,00				
0,11	4,02	244,99	84,40	982,97	3,42	3,42	0,00				
0,11	5,02	245,00	100,46	1228,16	3,41	3,41	0,00				
0,10	6,02	245,00	114,86	1472,48	3,40	3,40	0,00				
0,11	7,02	244,99	127,87	1717,67	3,39	3,39	0,00				
0,11	8,02	245,00	139,62	1963,74	3,38	3,38	0,00				
0,10	9,02	244,99	150,09	2207,16	3,37	3,37	0,00				
0,11	10,02	245,00	159,61	2453,24	3,36	3,36	0,00				
0,11	11,02	245,03	168,15	2698,45	3,35	3,35	0,00				
0,10	12,02	245,00	175,81	2942,77	3,35	3,35	0,00				
0,11	13,02	244,97	182,72	3187,95	3,34	3,34	0,00				
0,11	14,02	244,98	188,95	3433,12	3,33	3,33	0,00				
0,10	15,02	244,98	194,53	3677,41	3,33	3,33	0,00				
0,11	16,02	245,01	199,58	3922,60	3,32	3,32	0,00				
0,11	17,02	244,99	204,13	4168,68	3,31	3,32	0,00				
0,10	18,00	244,99	208,12	4207,70	3,31	3,31	0,00				
0,00	18,01	0,00	207,99	4409,46	3,65	3,63	-0,02				
0,21	20,01	0,00	168,54	4409,46	3,65	3,65	0,00				
0,21	22,01	0,00	136,57	4409,46	3,67	3,67	0,00				
0,21	24,01	0,00	110,63	4409,46	3,68	3,68	0,00				
0,21	26,01	0,00	89,65	4409,46	3,70	3,70	0,00				
0,21	28,01	0,00	72,64	4409,46	3,70	3,70	0,00				
0,21	30,01	0,00	58,82	4409,46	3,71	3,71	0,00				
0,21	32,01	0,00	47,66	4409,46	3,72	3,72	0,00				
0,21	34,01	0,00	38,62	4409,46	3,72	3,72	0,00				
0,21	36,01	0,00	31,27	4409,46	3,73	3,73	0,00				
0,21	38,01	0,00	25,34	4409,46	3,73	3,73	0,00				
0,21	40,01	0,00	20,54	4409,46	3,73	3,73	0,00				
0,21	42,01	0,00	16,63	4409,46	3,73	3,74	0,00				
0,21	44,01	0,00	13,48	4409,46	3,74	3,74	0,00				
0,21	46,01	0,00	10,92	4409,46	3,74	3,74	0,00				
0,21	48,01	0,00	8,84	4409,46	3,74	3,74	0,00				
0,21	50,00	0,00	7,17	4409,46	3,74	3,74	0,00				
0,01	50,05	-24,67	7,06	4408,80	3,76	3,77	0,01				
0,02	50,25	-97,44	5,66	4396,71	3,86	3,87	0,01				
0,02	50,45	-119,91	3,30	4375,19	3,89	3,90	0,01				
0,02	50,65	-124,44	0,66	4350,56	3,90	3,91	0,01				

Figure 4. FreedomCar battery parameter estimation spreadsheet [45].

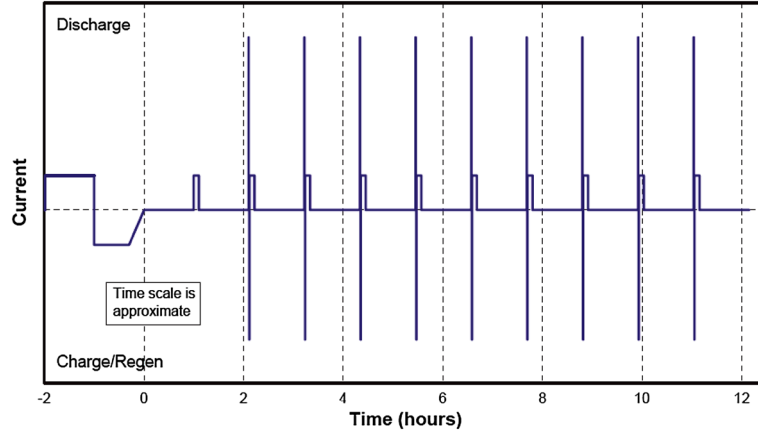


Figure 5. Hybrid pulse power characterization test [44].

- R_o : total ohmic resistance (Ω),
- C : polarization capacitor (F),
- I_p : polarization current (A),
- τ : time constant (s),
- I_b : battery current (A),

1.3.1.4. *Thévenin battery model*. Figure 6 represents a modified version of the FreedomCar battery model. This model is called the Thévenin battery model and it does not include the fictive capacitance 1/OCV'. As it is presented in Figure 6, the Thévenin model and the Freedomcar model (see Figure 3) assume the ohmic resistance of the battery during charging and discharging equal. However, in [10] is

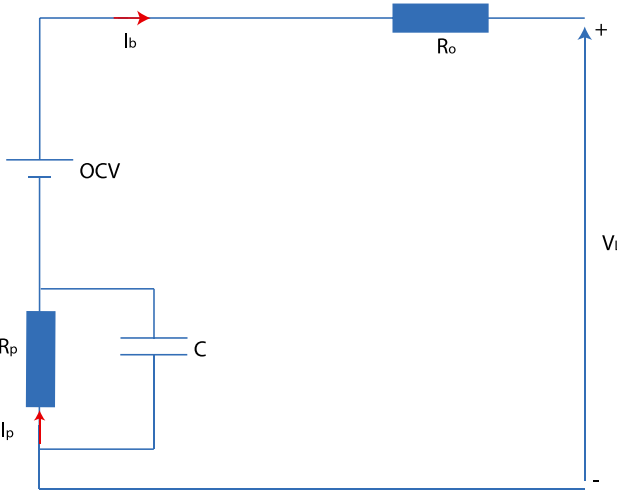


Figure 6. Thévenin battery model [44].

demonstrated that the charge and discharge resistances significantly differ. Moreover, the resistance varies with the SoC, temperature, current rate, and life cycle as reported in [10]. Equation (6) describes the Kirchoff voltage law of the Thévenin model.

$$V_L(t) = OCV(t) - R_o \cdot I_b(t) - R_p \cdot I_p(t) \quad (6)$$

In [47], an estimation tool has been developed for the estimation of the model parameters of the FreedomCar and Thévenin battery models. The tool is based on an iterative process, whereby the time constant of the model changes with a defined step time until a required fitting between the measurements data and the simulated data can be obtained. The fitted parameters are the OCV, ohmic resistance (R_o), the fictive capacitor ($1/OCV'$) and the polarization resistance, (R_p) and the time constant (τ). Here, it should be mentioned that the proposed tool is specifically designed for the FreedomCar and for the Thévenin battery models and is not suitable for a second-order or an RC or a complete any other battery model. Furthermore, the calculation time of this estimation tool is significantly long (few minutes for one charge and discharge HPPC pulse), which makes it unpractical.

1.3.1.5. Second-order FreedomCar battery model. The FreedomCar and the Thévenin battery models do not succeed in fitting the real battery characteristics at the end of charge or discharge phases [46]. In order to solve this problem, the FreedomCar battery model, which is a first-order model, can be extended up to second-order model (see Figure 7). The resistance R_{pa} demonstrates the activation polarization resistance, and R_{pc} represents the concentration polarization resistance with the respective capacitors C_{pa} and C_{pc} , which describe the transient response during power transfer from/to the battery. The general equation of the second-order FreedomCar battery model is presented in (7)

$$V_L(t) = OCV(t) - OCV'(t) \int I_b(t) \cdot dt - R_o \cdot I_b(t) - R_{p1} \cdot I_{p1} - R_{p2} \cdot I_{p2}(t) \quad (7)$$

where

- R_{pa} : activation polarization resistance (Ω),
- R_{pc} : concentration polarization resistance (Ω),
- C_{pa} : activation polarization capacitor (F),
- C_{pc} : concentration polarization capacitor (F),
- I_{p1} and I_{p2} : polarization current through the activation and concentration RC networks (A), and
- I_b : battery current (A).

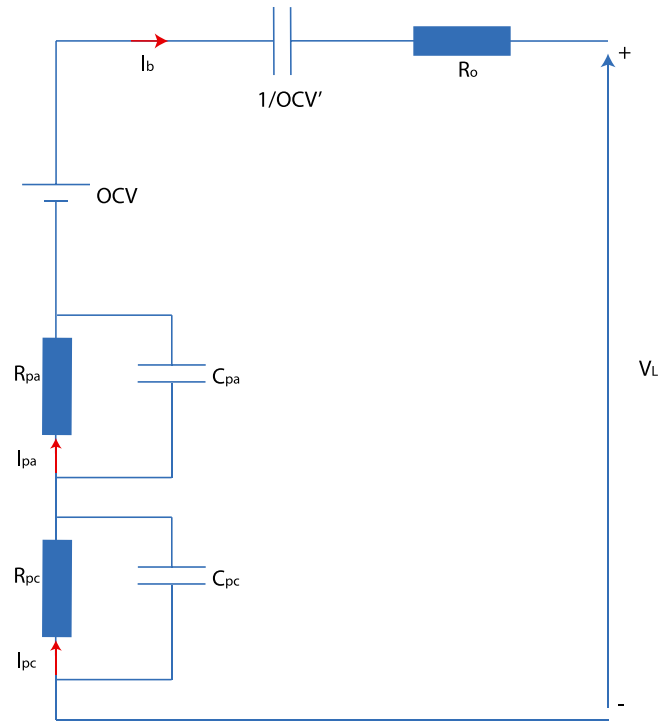


Figure 7. Second-order FreedomCar battery model [44].

The second-order FreedomCar battery model has the advantage that the battery behavior during the steady state and transient events better can be predicted, unlike with the Thévenin and first-order FreedomCar battery models.

1.3.1.6. Noshin's battery model. In the previous sections, several electrical battery models have been studied and analyzed, and their main characteristics are summarized. However, all those battery models have many drawbacks such as non-inclusions of the hysteresis effect, which has a significant impact on the battery performances, as presented by Figure 8. As can be seen in Figure 9, the nonlinearity of the battery models is not also taken into account (e.g., impacts of the discharge ohmic resistance during load) as reported in [10]. Furthermore, the OCV has been changed to be a variable parameter instead of a fixed value as presented by Figure 8. From the experimental results in Section 3, it is shown that the impact of the

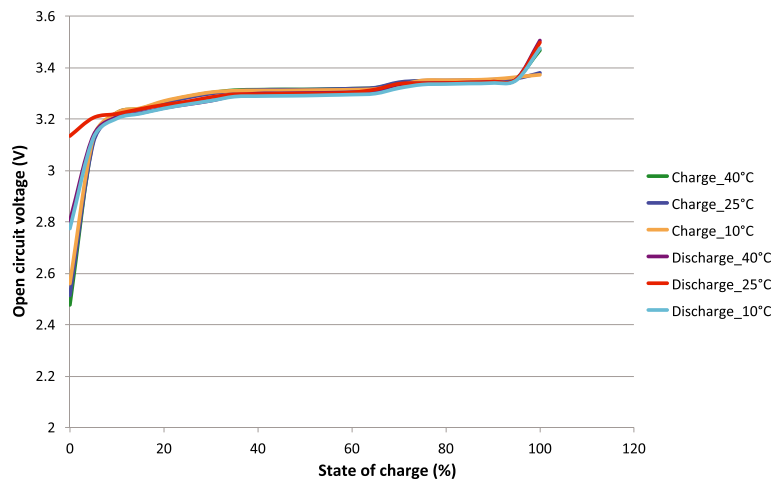


Figure 8. Hysteresis evolution based on cylindrical 2.3 Ah battery.

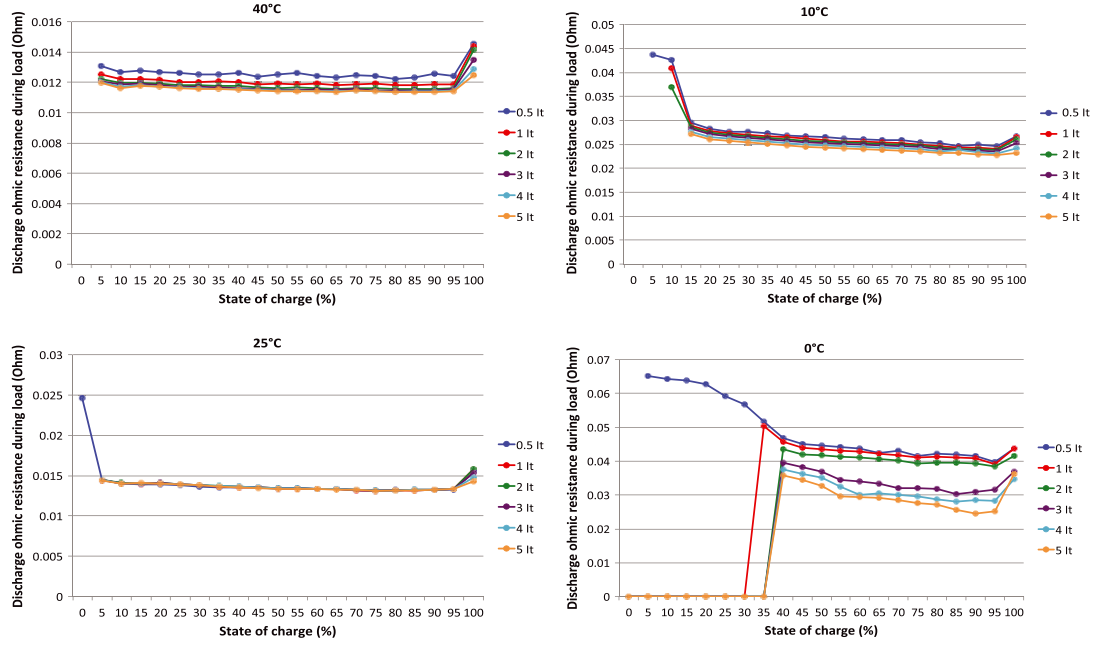


Figure 9. Evolution of the battery models parameters as function of state-of-charge, working temperature, and current rates.

variable parameters on the battery accuracy is considerably high. In addition, the estimation of the battery model parameters is based on the partnership for a new generation of vehicles spreadsheet, which is cumbersome and time-consuming. Thus, there is a need to develop a new battery model with a high accuracy for the BEVs and HEVs. This model contains the nonlinearity of the battery behavior, the required modifications, and an accurate/friendly technique for the estimation of the battery model parameters.

In [10], a new electrical battery model (extended Noshin's electrical battery model) has been proposed in order to illustrate the battery behavior more accurately (see Figure 10). This model has been derived on the basis of statistical data of the battery voltage evolution during charging and discharging of 30 types of

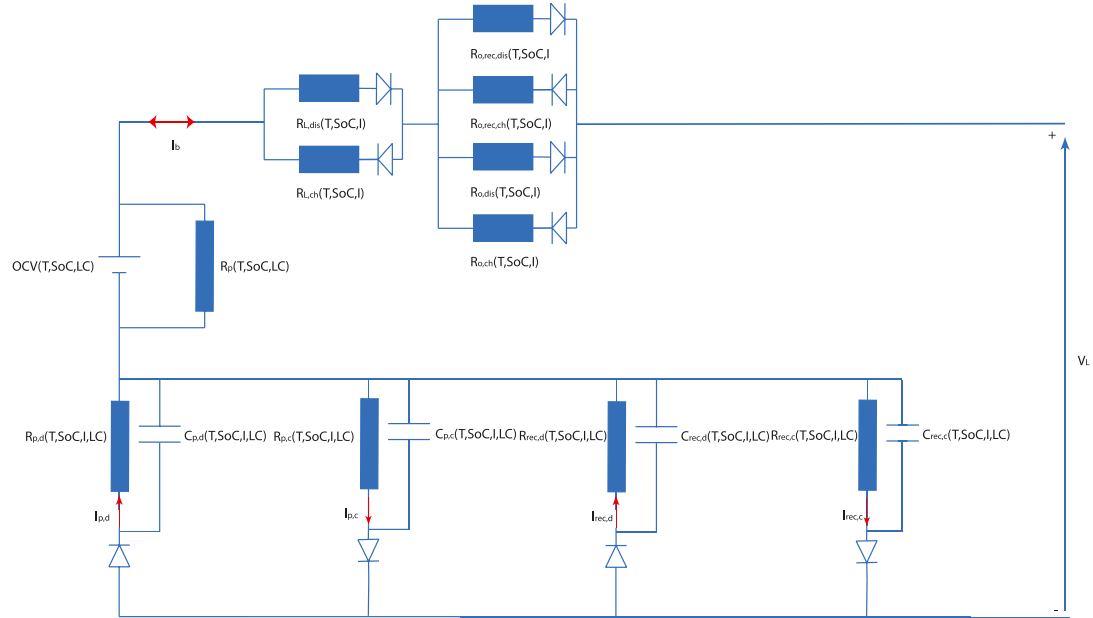


Figure 10. Extended Noshin's electrical battery model.

lithium-ion battery types (chemistries and sizes) at different working conditions such as state-of-charge and current rates. The performed analysis showed that the ohmic resistance of a battery cannot be considered as only one resistance as it is the case for the R_{int} , Thévenin, and FreedomCar battery models. Furthermore, the experimental results demonstrated the difference in the ohmic resistances ($R_{o,dis}$ and $R_{o,ch}$) when a load is imposed and ohmic resistance ($R_{o,rec,dis}$ and $R_{o,rec,ch}$) when the load decreases to zero. Moreover, the battery behaves different during the charging and discharging transition phenomena. In extended Noshin's battery model, this has been represented by two RC circuits ($R_{p,d}$ and $R_{p,ch}$). Two other RC branches ($R_{rec,d}$ and $R_{rec,ch}$) are also added to represent the polarization phenomena when the load decreases to zero. The model further features a self-discharge resistance (R_p) and internal resistances during charging and discharging because of the cycling of the battery ($R_{L,ch}$ and $R_{L,dis}$). The selection of the appropriate ohmic charge resistance ($R_{o,ch}$ and $R_{o,rec,ch}$) and ohmic discharge resistance ($R_{o,dis}$ and $R_{o,rec,dis}$) happens by using a dedicated logical algorithm.

It is noticed that this model significantly differs from other studied electrical battery models and has not been addressed in literature.

However, the fitting of the measurement data based on the extended Noshin's battery model at 1 I_t current rate and 90% SoC for the cylindrical 2.3 Ah battery type during the transitions (from full load to zero) is quite poor (85%) (as presented by Figure 11). The model has been adapted as presented in Figure 12, and the corresponding fitting of the measurement data based on the new adapted battery model at 1 I_t and

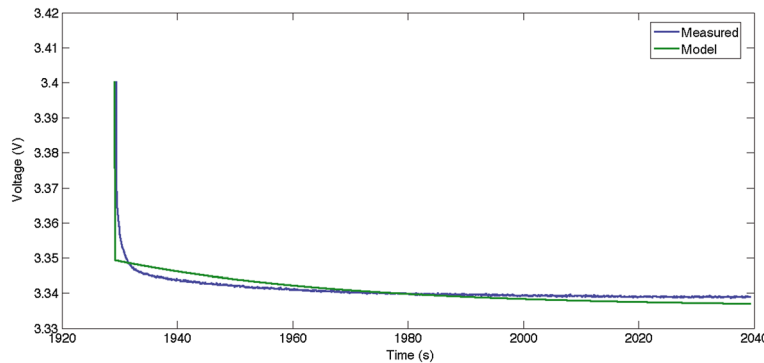


Figure 11. Comparison of the measured and fitted Noshin's battery model during steady-state conditions at room temperature, 1 I_t current rate and 90% SoC based on cylindrical 2.3 Ah battery type.

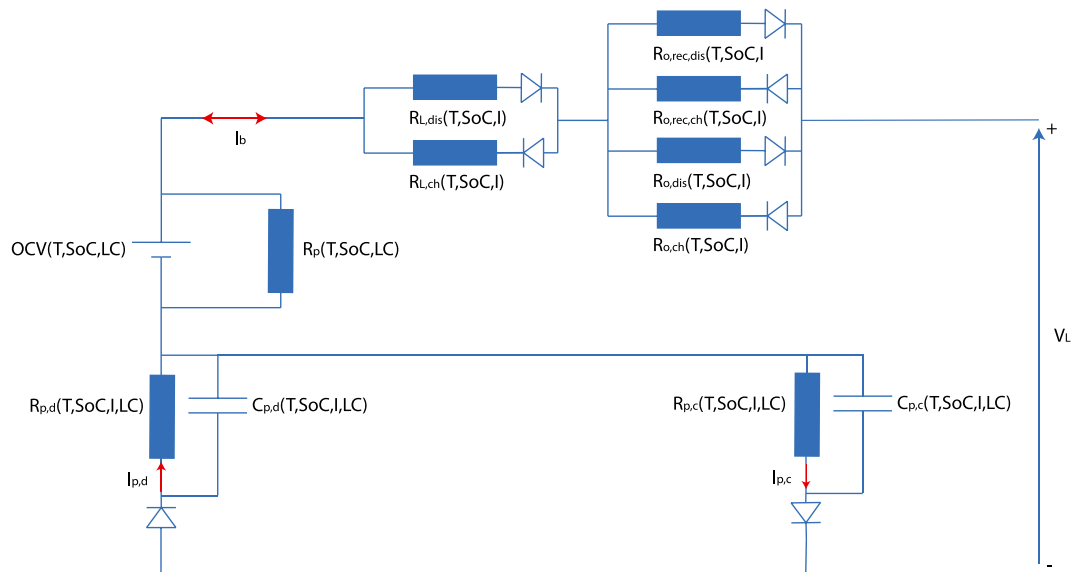


Figure 12. Noshin's electrical battery model.

90% SoC for the same battery type is about 99.7% as illustrated in Figure 13. In Figure 12, the model is defined as Noshin's battery model and will further be simulated and validated in this manuscript.

Here, it should be noted that the ohmic resistances ($R_{o,dis}$ and $R_{o,ch}$) have been calculated on the basis of Equations (8) and (9) as illustrated in Figure 14.

$$R_{o,ch} = \frac{U_1 - U_o}{I_b} \quad (8)$$

$$R_{o,dis} = \frac{U_2 - U_3}{I_b} \quad (9)$$

In Figure 14, the parameters U_{ch} and U_{dis} represent the maximum charge voltage and maximum discharge voltage during the pulse duration. The voltages U_1 and U_3 stand for the immediate voltage drop when a load is imposed to the battery. U_3 corresponds to sudden voltage drop when the current goes to zero. The voltages U_o and U_5 are the voltage at the beginning of the charge pulse and end of the discharge pulse when the voltage is stabilized.

1.3.1.7. Summary. The modeling of lithium-ion batteries can be divided into three main categories. The first group represents electrochemical modeling, where the main focus is to describe the electrochemical relationships.

These models are only suitable to illustrate or to investigate specific phenomena such as intercalation of lithium ions, heat transfer inside the electrolyte, and morphology of the electrodes [15,17–22,27,28,48].

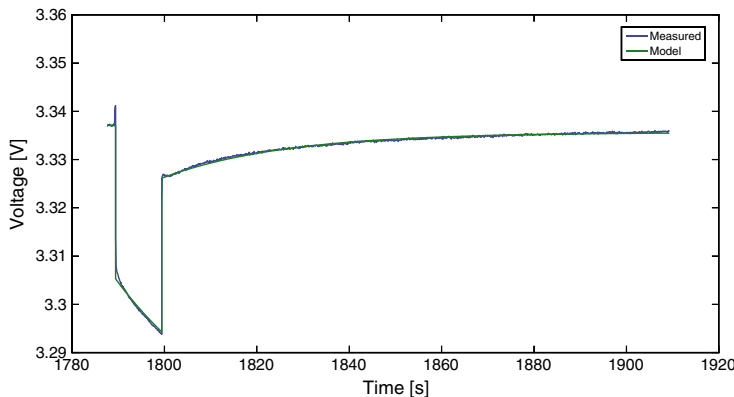


Figure 13. Comparison of the measured and fitted Modified Noshin's battery model during steady-state conditions at room temperature, 1 I_t current rate and 90% SoC based on cylindrical 2.3 Ah battery type.

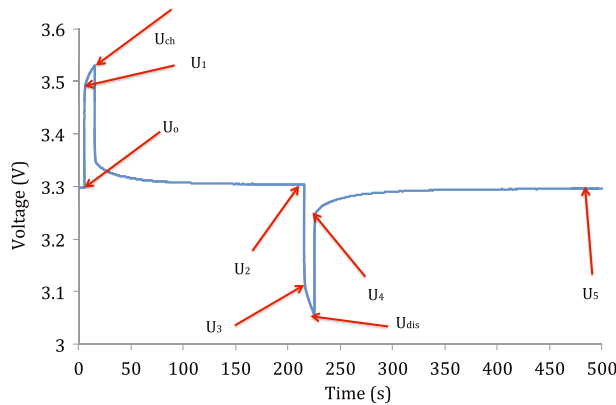


Figure 14. Evolution of the internal resistance during charge and discharge at 50% SoC and at room temperature for cylindrical 2.3 Ah battery type.

At laboratory level, the accuracy, which is strongly dependent of the estimated electrochemical parameters, could be very high. However, from the electrical point of view, these models are not suitable for PHEV applications.

The second group, the mathematical battery models, seems very similar to the electrochemical models. The mathematicians describe the various phenomena in the battery by sophisticated relationships. The mathematical equations that are used are mostly on the basis of differential equations of second or higher orders [31–33,35,37,38]. In order to reach a high accuracy, these models need significant amounts of data and chemical relationships, which can only be derived by specialized electrochemists. So, these models are also not appropriate to be used in PHEVs. As reported in [10,13,49], the BMS in PHEVs requires an electrical model for the prediction of the battery behavior. Such a model, consisting of electrical components such as capacitors, resistances, diodes, and voltage sources represent the most suitable solution. The electrical parameters of these models can be extracted by performing dedicated characterization tests as described in [11,12] without the need to access the innards of the battery cell.

From the point of view of the BMS in PHEVs, the electrical battery models are thus the most suitable solution as can be seen in Table I. Further, the electrical models are not complicated compared with the electrochemical and mathematical battery models, and their accuracy is relatively high.

2. EXTENDED LEVENBERG–MARQUARDT BATTERY MODEL MINIMIZATION TOOL

In the previous sections, a number of battery models have been compared and analyzed.

The estimation of the model parameters can be performed using mathematical equations as described in [10]. However, this methodology is time consuming and ineffective. Therefore, many estimation tools have been developed for battery modeling issues. One of these systems has been developed in [50]. The tool is based on the MATLAB/Simulink parameter estimation system. According to [51], the system is very powerful and can be implemented in any BMS structure. However, the system has some drawbacks such as long estimation time (several minutes) [51]. From third-order battery models, the systems block out [51].

The least squares method has been used for parameter estimation in a number of references [47,50,52]. This technique is well-adapted for fitting of linearized functions in parameters; because of the fact that a battery is a complex system, we can conclude however that there is a need for a more dedicated estimation technique, which can be used especially for lithium-ion-based batteries.

In the literature, one can find a number of fitting methods for fitting of nonlinear systems, such as the Gauss–Newton method (GNM) [53], which uses the quadratic nature of the cost function (CF) [53]. These algorithms attempt to minimize the CF between the calculated data y_{sim} and measured data y_{meas} as illustrated in Equation (10). Here, it should be noted that this technique finds the optimum parameter increment via a linear least squares minimization.

Another nonlinear minimization technique (gradient descent method (GDM)) uses variable incremental steps in the direction of the negative gradient of the CF for reaching the local optimum of the parameters [54]. This method seems very fast when the parameters are far of the local optimum.

$$CF = \frac{1}{2} \sum_{t=0}^{t=t_{\max}} [y_{\text{meas}}(t) - y_{\text{sim}}(t)]^2 \quad (10)$$

where

- CF: cost function,
- y_{sim} : simulated data,
- y_{meas} : measured data.

Table I. Comparison of different battery models [15,17–21,27,29–31,33–40,43–47].

Model	Complexity	Applicability in BMS	Accuracy
Electrochemical	—	—	High
Mathematical	—	—	High
Electrical	+	+	High

The Levenberg–Marquardt (LVM) method is a well-known minimization technique for solving of nonlinear least squares problems and it combines the GDM and GNM [53,54]. It is more robust and the (local) optimal solution can be found very fast. When the parameters are far from the local minimum, the LVM resembles the GDM, whereas when the parameters are near to the local minimum, the algorithm resembles the GNM. By combination, these two methods, the local minimum function will be reached very fast and accurately.

Parameter estimation relies on the minimization of the quadratic cost function, and the optimum parameters are the values, which minimize the cost function as formulated below:

$$\theta^* = \operatorname{argmin} \frac{1}{2} \sum_{t=0}^{t=t_{\max}} [y_{\text{meas}}(t) - f(I_b(t), \theta)]^2 \quad (11)$$

In Equation (11), $f(I_b(t), \theta)$ is the battery model voltage or simulated voltage, which takes in the terminal current and model parameters as arguments. Here, θ is a vector consisting of the battery model parameters (such as OCV, ohmic resistance (R_o), polarization resistance (R_p), time constant (tau)), and θ^* is the optimum parameter vector that minimizes the cost function defined in Equation (10).

A general drawback of a nonlinear least squares problem is that, unless the CF is convex, it can have many local minima and therefore several optimum solutions exist which depend on the initial set of starting parameter values. It was observed that the sensitivity of the CF to the initial parameter increased with the order of the model. Therefore, to ensure that the local optimum parameter is acceptable, based on the measurement data and an initial set of parameters, the LVM determines a local set of optimum model parameters θ^* . If all the parameters are non-negative and based on this θ^* , the fitting percentage achieves a desired value of 99%, this point is then accepted as the local optimum, but when the fitting value is lower than the desired, the initial starting value of the time constant(s) (tau) of the model is increased and re-optimized until the desired fitting percentage is achieved as presented in Figure 15. If the desired fitting percentage cannot be obtained, then the estimation technique will extract the model parameters based on the best local optimum point.

Because the nonlinear systems (such as batteries) may feature several optimal points, it was observed that the performance of the algorithm was most sensitive to the starting value of model's time constants. Whereby for a set of different starting-time constants and the remaining parameters unchanged, either the value of the CF increased or the optimized parameters ended up being negative. By reinitializing with the time constant incremented by an arbitrary small value, the final optimized parameters became positive and the CF improved. The sensitivity further increased with the order of the model.

As such with initially small starting time constants (0.1 s), the values are incremented if the resulting optimized parameters are negative or if the CF increases. A flowchart for the parameter estimation employed in this work is shown in Figure 15.

Note that in the flowchart shown in Figure 15, the procedure can be made to terminate or exit the loop by setting an upper bound to the time constants.

In Figure 16, an example of the fitted second-order FreedomCar battery model and measurements is demonstrated. One can observe from Figure 16, a good agreement between the simulated and the model results is achieved. According to Figure 16, the fitting percentage is around 99.8%.

In Table II, an overview of the fitting between the simulated battery models and experimental data is presented. As one can observe, the fitting percentage of the investigated battery models based on the advanced LVM minimization tool is high.

3. RESULTS AND DISCUSSIONS

3.1. Validation of the electrical battery models

In this section, the R_{int} , RC, Thévenin, first FreedomCar, second, third FreedomCar orders, and Noshin's battery model as presented in Figure 12 have been simulated on the basis of the extended LVM minimization tool and validated at different working conditions.

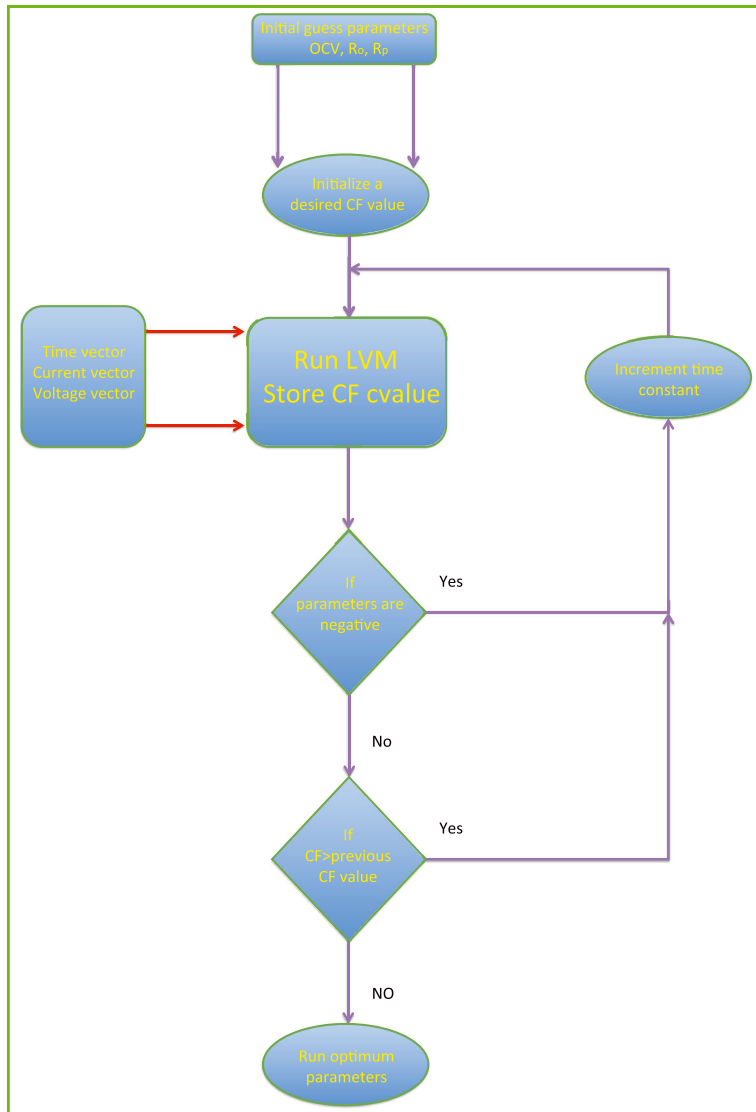


Figure 15. Optimization flow chart of optimized Levenberg–Marquardt minimization tool.

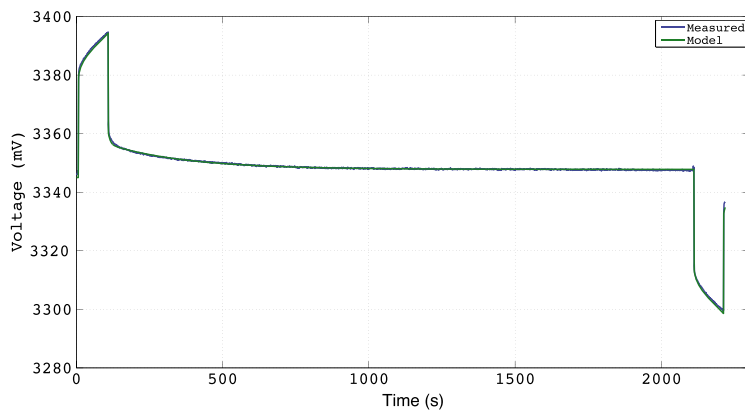


Figure 16. Comparison of measured and fitted second-order FreedomCar battery model at room temperature-based, 1 I_t and 90% SoC based on cylindrical 2.3 Ah battery type.

Table II. Fitting percentage of the investigated battery models at 50% SoC, 1 I_t current rate and at room temperature.

Battery model	Fitting (%)
R_{int}	99.8
RC	99.7
Thévenin	99.8
First-order FreedomCar model	99.8
Second-order FreedomCar model	99.9
Third-order FreedomCar model	99.8
Noshin's battery model	99.8

In this paper, a cylindrical LFP battery cell with rated capacity 2.3 Ah has been used for a validation analysis.

For calibration of the aforementioned battery models, the extended HPPC test at room temperature, as documented in [10], has been used from 100% to 0% SoC with steps of 5%. This is needed because of the nonlinear characteristics of the proposed battery type in the SoC regions (100–95%) and (10–0%) as reported in [10].

In this section, the battery models have been validated at different load profiles as presented. The following tests have been carried out at room temperature (20–25 °C):

- (1) The first test is a pulse test where the battery cell is completely charged (constant current at 1 I_t and during constant voltage (3.6 V) until the battery current is reduced till 0.01 I_t) and then discharged with pulses of 2 I_t during 10 s until the cut-off voltage (2 V) is reached. After charging and discharging, a rest time of 30 min has been implemented in order to stabilize the battery voltage.
- (2) The second test represents the dynamic discharge performance test as presented in [11,12].
- (3) In order to validate the battery models at constant currents, the model performances have been compared at 1 I_t and 5 I_t constant discharge currents. In this test, the same charge procedure as in the previous tests has been used.

In order to compare the accuracy of the different battery models as accurately as possible, the maximum error percentage of the battery models has been summarized in the DoD regions 0–5%, 5–90%, and 90–100% (see Tables III–V). The bold red values represent the best battery model accuracy for the corresponding test.

The accuracy of the model has been derived on the basis of Equation (12)

$$\text{Error} = \frac{\text{Voltage}_{\text{experimental}} - \text{Voltage}_{\text{model}}}{\text{Voltage}_{\text{experimental}}} \cdot 100\% \quad (12)$$

All measures have been performed by using the battery tester SBT 0550 from company PEC corporation [10].

3.1.1. Depth of discharge window: 0–5%. In Table III, one can generally observe that all the battery models have difficulties to predict the battery behavior in the depth of discharge region 0–5%. The

Table III. Comparison of the error expressed in percent sign of the battery models in the DoD range 0–5% at room temperature (measurement error: 0.5%).

Model	Pulse test (%)	Dynamic Discharge Performance test (%)	Capacity test at 1 I_t (%)	Capacity test at 5 I_t (%)
R_{int}	4.5	5.0	3.0	8.0
RC	8.0	5.0	7.0	6.0
Thévenin	3.5	4.0	2.0	2.0
First FreedomCar	2.0	4.0	2.0	6.0
Second FreedomCar	2.0	2.5	2.0	4.0
Third FreedomCar	1.5	3.0	2.0	3.0
Noshin's battery model	2.0	2.5	2.0	2.0

Table IV. Comparison of the error expressed in percent sign of the battery models in the DoD range 5–90% at room temperature (measurement error: 0.5%).

Model	Pulse test (%)	DDP test (%)	Capacity test at 1 I_t (%)	Capacity test at 5 I_t (%)
R_{int}	7.0	15.0	5.0	9.0
RC	2.0	5.0	2.0	5.0
Thévenin	5.0	4.0	1.0	7.0
First FreedomCar	1.5	3.5	1.5	12.0
Second FreedomCar	2.0	2.0	2.0	14.0
Third FreedomCar	2.0	1.0	2.0	12.0
Noshin's battery model	1.5	3.0	1.0	2.0

Table V. Comparison of the error expressed in percent sign of the battery models in the DoD range 90–100% at room temperature (measurement error: 0.5%).

Model	Pulse test (%)	DDP test (%)	Capacity test at 1 I_t (%)	Capacity test at 5 I_t (%)
R_{int}	14.0	20.0	18.0	19.2
RC	55.0	46.0	58.0	50.0
Thévenin	17.0	15.0	20.0	19.0
First FreedomCar	25.0	19.0	29.0	18.0
Second FreedomCar	19.0	14.0	25.0	35.0
Third FREEDOMCAR	17.0	13.0	23.0	28.0
Noshin's battery model	13.5	14.0	16.5	12.5

error percentage varies for all the models between 1.5% and 6.0% with exception of the battery models R_{int} and RC, where the error is slightly higher, 3.0–8.0%. In Table III, one can conclude that the performances of Noshin's battery model are much better than the second and third-order FreedomCar battery models. The error for the new battery model varies between 2.0% and 2.5%.

3.1.2. Depth of discharge window: 5–90% DoD. The DoD region 5–90% shows a big variation between the different battery models. Particularly for the R_{int} battery model, the error percentage is significantly higher at 5.0–15.0%. Moreover, at 5 I_t current rate, the different battery models have difficulties to predict the battery behavior accurately with the exception of Noshin's battery model. The error is 2.0% compared with 5.0–24.5% for another battery models.

In Table IV, it is noticeable that the error percentage for the RC battery model is significantly smaller (2.0–5.0%). This due to the linear decrease of the battery voltage, which matches the real battery behavior of the investigated battery type in the selected DoD range as reported in [10].

3.1.3. Depth of discharge window: 90–100% DoD. Table V considers the 90–100% DoD range. The battery models show an error percentage between 13.5% and 58%. However, Noshin's battery model and third-order FreedomCar models give the best results.

But here, it should be noted that Noshin's battery model has better performances than the third-order FreedomCar battery model despite its lower order.

Furthermore, it is remarkable that the RC battery model shows the worst performances. The high error percentage of the RC battery is because the battery model as presented in Figure 2 can be interpreted as the parallel combination of a battery cell and a large capacitor cell. The left part of the model represents a battery, and the right part stands for the capacitor. In addition, the battery model assumes that the model parameters are fixed and do not change in function of the SoC. Therefore, the battery voltage decreases linearly as a function of depth of discharge. This is typical for a capacitor and similar to the electrical double-layer capacitor evolution during discharging as demonstrated in [10].

In order to increase the accuracy of the battery model behavior in the DoD region 90–100%, the HPPC test should be carried out every 2% DoD. This is needed to cover better the nonlinear behavior of the battery in this region. Furthermore, the models' behavior can be enhanced (5.0–10%) using

polynomial interpolation relationships between the data points in the look-up tables or neural networking techniques instead of linear interpolation, as is the case for the MATLAB/Simulink look-up tables.

3.2. Validation of Noshin's battery model at different operating temperatures

In the previous sections, the various battery models have been validated and compared. From the analysis, one can conclude that Noshin's battery model that has been proposed in this paper has better performances than the other investigated battery models. In order to assess the battery performances at different operating temperatures, the pulse test has been repeated at the working temperatures 40 °C and 0 °C. Prior to starting with the validation tests, Noshin's battery model has been calibrated on the basis of the extended HPPC test at 40 °C and 0°C as demonstrated by Figure 9 (e.g., evolution of the discharge ohmic resistance during load at different SoC, current rates, and working temperatures).

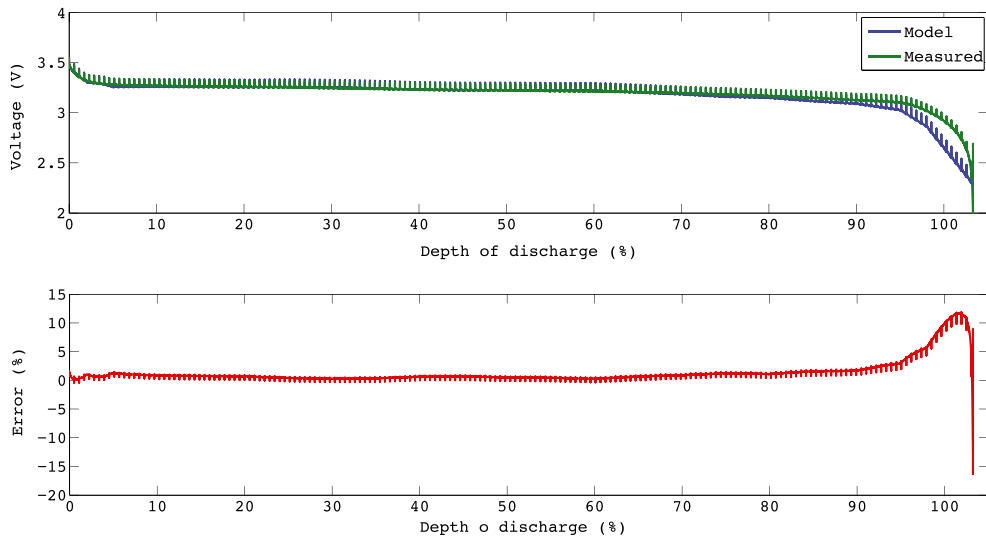


Figure 17. Comparison of the simulation and experimental results of Noshin's battery model at 40 °C operating temperature (error: 0.5%).

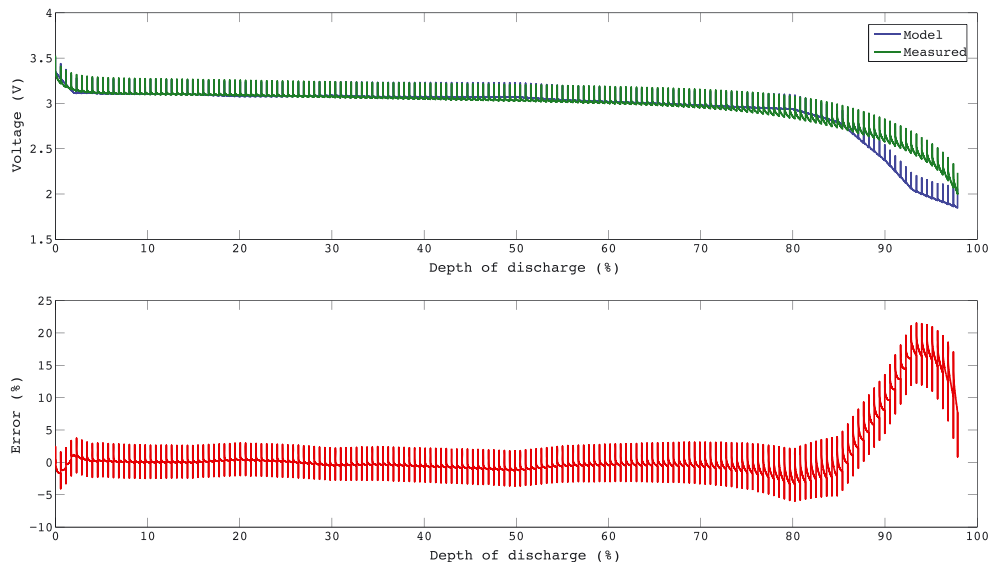


Figure 18. Comparison of the simulation and experimental results of Noshin's battery model at 0 °C operating temperature (error: 0.5%).

In Figure 17, one can observe that Noshin's battery model is in a good agreement with the experimental results. The error percentage in the DoD range 0–90% is smaller than 1.5%. However, from 90% DoD and higher, the model is not able to predict the battery behavior accurately. The maximum error percentage is about 17%. In Figure 18, the situation is illustrated at 0 °C operating temperature. Here, we can conclude that the error is slightly higher (5%) in the DoD range 0–90% than the test at 40 °C. The main reason therefore is that the fitting of the model parameters at 0 °C does not perform very well as at 40 °C or 25 °C.

4. SUMMARY AND CONCLUSIONS

In this paper, a number of battery models have been studied and compared on the basis of the optimized minimization technique called extended Levenberg–Marquardt on battery model parameters.

This technique has been applied on various battery models such as the R_{int} , RC, Thévenin, first, second, and third FreedomCar battery models and Noshin's battery model that was proposed in [10] and further optimized in this paper as presented by Figure 12.

The extended Levenberg–Marquardt battery estimation tool is able to predict the battery model parameter very precisely (99.8%).

The performed analysis showed that Noshin's electrical battery model can predict the battery behavior better than the other mentioned battery models. The model accuracy varies between 2% and 3%, 1% and 3%, 13.5% and 16.5% in the DoD ranges (0–5%), (5–90%), and (90–100%) compared with 2–4%, 2–14%, and 13–28% for the second-order FreedomCar battery model in the same DoD ranges. These results have been derived on the basis of validation of the models at different load profiles and at room temperature conditions.

Moreover, Noshin's battery model has been validated at 40 °C and 0 °C working temperatures. The accuracy of the model is smaller than 1.5% and 5% at 40 °C and 0 °C, respectively. The latter results are based on the depth of discharge range (0–90%).

5. LIST OF ABBREVIATIONS

BEV	Battery electric vehicle
BMS	Battery management system
C_b	Bulk capacitor
C_c	Surface capacitor
CF	Cost function
C_{pa}	Activation polarization capacitor
C_{pc}	Concentration polarization capacitor
DDP	Dynamic discharge performance
DoD	Depth of discharge
GDM	Gradient descent method
GNM	Gauss-newton method
HEV	Hybrid electric vehicles
HPPC	Hybrid pulse power characterization
I_b	Battery current
I_p	Polarization current
I_t	Reference current
LFP	Lithium iron phosphate
LVM	Levenberg–Marquardt
OCV	Open circuit voltage
OCV'	Fictive capacitor
PHEV	Plug-in hybrid electric vehicle
R	Resistance
RC	Resistor-capacitor

R_c	Resistance in series with capacitor C_c
R_{ch}	Charge resistance
R_{co}	Ohmic charge resistance
R_d	Discharge resistance
R_{do}	Ohmic discharge resistance
R_e	Resistance in series with the capacitor C_b
$R_{L,ch}$	Charge resistance during cycle life
$R_{L,dis}$	Discharge resistance during cycle life
R_o	Ohmic resistance
$R_{o,ch}$	Ohmic charge resistance
$R_{o,dis}$	Ohmic discharge resistance
$R_{o,rec,ch}$	Ohmic charge resistance when the load decreases to zero
$R_{o,rec,dis}$	Ohmic discharge resistance when the load decreases to zero
R_p	Polarization resistance
$R_{p,ch}$	Polarization charge resistance
$R_{p,d}$	Polarization discharge resistance
R_{pa}	Activation polarization resistance
R_{pc}	Concentration polarization resistance
$R_{rec,ch}$	Polarization charge resistance when the load decreases to zero
$R_{rec,d}$	Polarization discharge resistance when the load decreases to zero
R_t	Represents the resistance of the connection between the two RC circuits
SoC	State of charge
T	Time vector
τ	Time constant
U_{ch}	End of the charge voltage
U_{dis}	End of the discharge voltage
V_{cb}	Voltage of the capacitor C_b
V_{cc}	Voltage of the capacitor C_c
V_L	Battery voltage

REFERENCES

- IEA (International Energy Agency). *Energy Technology Perspectives – Scenarios and Strategies to 2050*. OECD Publishing: Paris, France, 2008.
- Van Mierlo J, Maggetto G. Comparison of the environmental damage caused by vehicles with different alternative fuels and drive trains in a Brussels context. *Journal of Automobile Engineering* 2003; **36**:583–593.
- Boureima FS. Environmental assessment of conventional and alternative vehicles and fuels in a Belgian context. *PhD Thesis*, Vrije Universiteit Brussel, Brussels, Belgium, September 2011.
- Axsen J, Kurani KS, Burke A. Are batteries ready for plug-in hybrid buyers? *Journal of Transport Policy* 2010; **17**:173–182.
- Van den Bossche P, Vergels F, Van Mierlo J, Matheys J, Van Autenboer W. SUBAT: an assessment of sustainable battery technology. *Journal of Power Sources* 2006; **162**:913–919.
- Omar N, Daowd M, Mulder G, Timmermans JM, Van Mierlo J, Pauwels S. Assessment of performance of lithium ion phosphate oxide, nickel manganese cobalt oxide and nickel cobalt aluminum oxide based cells for using in plug-in battery electric vehicle applications. *International Conference Vehicle Power and Propulsion Conference*, Chicago, USA, September 6–9, 2011.
- Omar N, Verbrugge B, Mulder G, et al. Evaluation of performance characteristics of various lithium-ion batteries for use in BEV application. *International Conference Vehicle Power and Propulsion Conference*, Lille, France, September 1–3, 2010.
- Omar N, Daowd M, Verbrugge B, et al. Assessment of performance characteristics of lithium-ion batteries for PHEV vehicles applications based on a newly test methodology. *The 25th International Conference on Battery, Hybrid and Fuel Cell Electric Vehicle*, Shenzhen, China, November 5–8, 2010.
- Burke A, Miller M. Performance characteristics of lithium-ion batteries of various chemistries for plug-in hybrid vehicles. *The 24th International Conference on Battery, Hybrid and Fuel Cell Electric Vehicle*, Stavanger, Norway, May 13–16, 2009.
- Omar N, Van den Bossche P, Daowd M, et al. Rechargeable energy storage systems for plug-in hybrid electric vehicles - assessment of electrical characteristics. *Energies* 2012; **5**:2952–2988.

11. Omar N, Daowd M, Hegazy O, et al. Standardization work for BEV and HEV applications: critical appraisal of recent traction battery documents. *Energies* 2012; **5**:138–156.
12. Mulder G, Omar N, Pauwels S, et al. Enhanced test methods to characterise automotive battery cells. *Journal of Power Sources* 2011; **196**:10079–10087.
13. Daowd M, Omar N, Van den Bossche P, Van Mierlo J. A review of passive and active battery balancing based on MATLAB/Simulink. *Journal of International Review of Electrical Engineering-IREE* 2011; **6**:2974–2989.
14. Ershag OA. Balancing and monitoring system for battery cell stacks in electrical vehicles. *Master's Thesis*, Lulea University of Technology, Strömsund, Sweden, June 2008.
15. Ning G, Haran B, Popov BN. Capacity fade study of lithium-ion batteries at high discharge rates. *Journal of Power Sources* 2003; **117**:160–169.
16. Bloom I, Cole BW, Sohn JJ, et al. An accelerated calendar and cycle life study of li-ion cells. *Journal of Power Sources* 2001; **101**:238–247.
17. Deiss E, Häring D, Novak P, Haas O. Modeling of the charge–discharge dynamics of lithium manganese oxide electrodes for lithium-ion batteries. *Electrochimica Acta* 2001; **46**:4185–4196.
18. Karthikeyan DK, Sikha G, White RE. Thermodynamic model development for lithium intercalation electrodes. *Journal of Power Sources* 2008; **185**:1398–1407.
19. Jossen A. Fundamentals of battery dynamics. *Journal of Power Sources* 2006; **156**:530–538.
20. Ménard L, Fontès G, Astier S. Dynamic energy model of a lithium battery. *Journal of Mathematics and Computers in Simulation* 2010; **81**:327–339.
21. Santhanagopalan Sh, Guo Q, Ramadass P. Review of models for predicting the cycling performance of lithium ion batteries. *Journal of Power Sources* 2006; **156**:620–628.
22. Baert D, Vervaet A. Lead-acid battery model for the derivation of Peukert's law. *Electrochimica Acta* 1999; **44**:3491–3504.
23. Zadin V, Brandell D, Notten D, Aabloo A. Finite element simulations of 3d ionic transportation properties in li-ion electrolytes. *Electrochimica Acta* 2012; **65**:165–173.
24. Danilov D, Nessen R, Notten R. Modeling all-solid-state li-ion batteries. *Journal of Electrochemistry Society* 2010; **158**:A215–A222.
25. Danilov D, Notten D. Li-ion electrolyte modeling: the impact of adding supportive salts. *Journal of Power Sources* 2008; **189**:303–308.
26. Danilov D, Notten D. Mathematical modeling of ionic transport in the electrolyte of li-ion batteries. *Electrochimica Acta* 2008; **53**:5569–5578.
27. Dees D. Electrochemistry cell model. *Electrochemical Energy Storage Chemical Sciences and Engineering Divison*, May 2009.
28. Christensen J, Newman J. Effect of anode film resistance on the charge/discharge capacity of a lithium-ion battery. *Journal of Power Sources* 2003; **150**:A1416–A1420.
29. Newman J, Thomas-Alyea KE. *Electrochemical Systems*, 3rd edn. John Wiley & Sons, 2004. ISBN: 978-0-471-47756-3
30. Barsoukov E, Macdonald JR. *Impedance Spectroscopy: Theory, Experiment, and Applications*, 2nd edn. John Wiley & Sons, 2005. ISBN-10: 0471647497.
31. Botte GG, Subramanian VR, White R. Mathematical modeling of secondary lithium batteries. *Electrochimica Acta* 2000; **45**:2595–2609.
32. Rakhamatov D, Vrudhula S. An analytical high-level battery model for use in energy management of portable electronic systems. *International Conference on Computer Aided Design*, California, USA, November 2001.
33. Rakhamatov D, Vrudhula S. Battery lifetime predictions for energy-aware computing. *International Symposium on Low Power Electronics and Design*, California, USA, August 2003.
34. Fan D, White RE. Mathematical modeling of a nickel-cadmium battery - effects of intercalation and oxygen reactions. *Electrochimica Acta* 1991; **138**:2952–2960.
35. Polyakov IO, Dugaev VK, Kovalyuk ZD. Simulation of lithium battery discharge. *Journal of Electrochemistry* 1997; **33**:26–30.
36. Rong P, Pedram M. An analytical model for predicting the remaining battery capacity of lithium-ion batteries. *IEEE Transactions on Very Large Scale Integration Systems* 2006; **14**:441–451.
37. Manwell JF, McGowan JG. Lead acid battery storage model for hybrid energy systems. *Journal of Solar Energy* 1993; **50**:399–405.
38. Manwell J, McGowan J. Evaluation of battery models for wind/hybrid power system simulation. *5th European Wind Energy Association Conference*, Thessaloniki, Greece, 1994.
39. Tremblay O, Dessaint LA, Dekkiche A. A generic battery model for the dynamic simulation of hybrid electric vehicles. *International Conference Vehicle Power and Propulsion Conference*, Texas, USA, September 2007.
40. Zhang H, Chow MY. Comprehensive dynamic battery modeling for PHEV applications. *Power and Energy Society General Meeting*, Detroit, USA, July 2010.
41. Durr M, Cruden A, Gair S, McDonald JR. Dynamic model of a lead acid battery for use in a domestic fuel cell systems. *Journal of Power Sources* 2006; **161**:1400–1411.
42. Barsali S, Cerciaoli M. Dynamical models of lead- acid batteries: Implementation issues. *IEEE Transactions on Energy Conversion* 2002; **17**:16–23.
43. Tang Y. On the feasibility of hybrid battery/ultracapacitor energy storage systems for next generation shipboard power systems. *International Conference Vehicle Power and Propulsion Conference*, Lille, France, September 2010.

44. Wipke K, Cuddy M, Bharathan D, *et al.* Advisor 2.0: a second-generation advanced vehicle simulator for systems analysis. Technical Report Contract No. DE-AC36-98-GO10337, NREL, 1999.
45. Johnson VH, Pesaran A, Sack Th. Temperature-dependent battery models for high-power lithium-ion batteries. *The 17th International Conference on Battery, Hybrid and Fuel Cell Electric Vehicle*, Montréal, Canada, October 2000.
46. FreedomCAR battery test manual for IDAHO. U.S. Department Secretary of Energy, 2003.
47. Verbrugge B, Heremans Y, Van Mulders F, Culcu H, Van den Bossche P, Van Mierlo J. Modelling the RESS: describing electrical parameters of batteries and electric double-layer capacitors through measurements. *World Electric Vehicle Journal* 2009; **3**:2032–6653.
48. Bard L, Faulkner L. *Electrochemical Methods: Fundamentals and Applications*. Kluwer Academic/Plenum, 2011. ISBN: 0-471-04372-9
49. Su-Ming Fan B. Modeling and simulation of a hybrid electric vehicle using MATLAB/Simulink and Adams. *Master thesis*, University of Waterloo, 2007.
50. Jackey RA, Plett GL, Klein MJ. Parameterization of a battery simulation model using numerical optimization methods. *SAE World Congress Exhibition*, Thessaloniki, Greece, January 2009.
51. Daowd M, Omar N, Van den Bossche P, Van Mierlo J. An extended pmvg battery model for electric and hybrid vehicles. *International Review of Electrical Engineering-IREE* 2011; **6**:1692–1706.
52. Björck A. Numerical methods for least squares problems, volume I of 0-89871-360-9, 1996.
53. Marquardt D. An algorithm for least-squares estimation of nonlinear parameters. *Journal of Society for Industrial and Applied Mathematics* 1963; **11**:431–441.
54. Lourakis M. A brief description of the Levenberg–Marquardt algorithm implemented by levmar. *Technical Report*, Institute of Computer Science, Foundation for Research and Technology - Hellas, 2005.